Australian Government

Department of Defence

Defence Science and
Technology Organisation

Application of the Fractional Fourier Transform in the Detection of Accelerating Targets in Clutter

R. Melino and H.T. Tran

Electronic Warfare and Radar Division

Defence Science and Technology Organisation

ABSTRACT

We demonstrate that the Fractional Fourier transform is a very efficient and practical technique for detecting accelerating targets in both land and sea clutter, where the traditional Fourier transform method may fail.

APPROVED FOR PUBLIC RELEASE

APPROVED FOR PUBLIC RELEASE

Application of the Fractional Fourier Transform in the Detection of Accelerating Targets in Clutter

Executive Summary

Accelerating targets introduce chirped signals in the radar backscatter signal which cannot be efficiently detected by the traditional Fourier transform (FT). However, they can appear as pure tone signals with the Fractional Fourier Transform (FrFT) and thus can be efficiently detected with the same coherent integration gain achievable by the FT on pure tone signals. The important feature allowing success of the FrFT is the achievable optimum focusing of chirped signals when applied to the FrFT, whereas the clutter signal is always defocused. Results achieved based on simulated clutter data have shown to be very promising.

THIS PAGE IS INTENTIONALLY BLANK

Contents

Figures

Tables

Glossary

CPI: Coherent Processing Interval

FrFT: Fractional Fourier Transform

LFM: Linear Frequency Modulated (signal)

PDF: Probability distribution function

SCR: Signal-to-Clutter Ratio

STFT: Short-Time Fourier Transform

THIS PAGE IS INTENTIONALLY BLANK

1   Introduction

The current work is focused on answering the question of how the relatively new tool called the Fractional Fourier Transform (FrFT) can be used to significantly improve the detection of an airborne accelerating target in the presence of land and sea clutter by a pulsed Doppler radar.

The use of the classic Fourier transform (FT) in coherent radars, for detection purposes, works most efficiently on constant (radial) velocity targets which impart pure tone signals in the radar backscatter. For accelerating targets inducing chirped signals, whose instantaneous frequency varies approximately linearly over a typical coherent processing interval (CPI)[1], a frequency line in the frequency spectrum would become spread out, the extent of which depends on the bandwidth of the induced chirps. Fortunately, the FrFT, which can be viewed as a generalisation of the traditional FT, can be used to achieve the same level of coherent integration gain, although with an extra but affordable computational throughput requirement. With the FrFT, chirp signals can appear as pure tone signals in 'fractional time', in a suitably rotated time-frequency domain. This is the first major advantage of using the FrFT.

The second advantage of using the FrFT is the possible defocussing, or suppression, of clutter signal power in the rotated (or 'fractional') frequency domain when the FrFT is applied to focus the chirped target signal. Some of the discussion in this work will be devoted to this effect, to determine how much radar clutter of various types can be suppressed at various angles of rotation of the time-frequency domain. Here, simulated clutter data has been used to demonstrate preliminary results. Further results on real clutter data will be reported at a later time.

To complete the discussion, we also review recent developments in the literature on the topic of accelerating target detection in clutter. In particular, the time-frequency techniques proposed by Yasotharan *et al.* [1] and other tools [2] such as the S-Method will be discussed and compared with the FrFT.

The main results from this work are as follows. We find that the FrFT is the most suitable technique when the Doppler profile of the accelerating target is either inside or significantly overlapping with that of clutter, while the S-Method is most efficient when target Doppler is close but sufficiently separated from the clutter Doppler region. The two techniques can thus be viewed as mutually complimentary, in the sense of maintaining detection of a manoeuvring air target for the whole duration of a manoeuvre in most realistic scenarios in which the target manoeuvres in and out of the clutter frequency region. The FrFT is slightly more computationally expensive but produces estimates for both the target velocity and target acceleration for the current CPI, while the S-Method is a slightly faster technique and produces only an average target velocity.

---

[1] A CPI is a time interval over which the signal is coherently integrated to maximise the signal gain in the receiver.

2   Radar Environment and Signal Models

Our current problem assumes an airborne pulsed Doppler radar, in a look-down scenario, with its receiver employing possibly a number of range bins and a CPI of N time samples, which is supposed to be both large enough to capture the acceleration of a target and short enough to be compatible with the baseline processing of the radar preventing 'range walk' across adjacent range bins. Furthermore,

- Detection processing is required at each CPI, and thus the choice of processing across the CPIs may be an additional option but not a replacement of the CPI-level processing;

- Each range bin is Doppler processed separately, using the same algorithms proposed herein.

- For simplicity, only schematic radar antenna gain patterns are currently included in our study.

Within this context, ground or sea clutter is expected to have a finite Doppler extent depending on the range bin being processed, antenna gain pattern and look angle, platform speed, and altitude. Signal data structures such as spectrograms are not involved, and only Doppler processing for a CPI needs be considered. For practical reasons, we also assume that no more than one accelerating target can be present in any one range bin and any one CPI.

In continuous form, the total signal in the radar receiver typically consists of three components

$$u(t) = s(t) + c(t) + n(t),$$

of the target signal itself, the clutter, and the receiver thermal noise, respectively. The thermal noise component $n(t)$ is assumed to be simply Gaussian white noise with its amplitude set to 10 dB below the clutter. The following subsections describe the models being used for $s(t)$ and $c(t)$ in some detail.

2.1   Target Model

Assuming that the target has a constant linear acceleration a during the CPI, the target velocity is $v = v_0 + at$, where v_0 is initial velocity. In the monostatic radar configuration, the sampled radar return signal from the target can readily be shown to take the form

$$s(t_n) = A_n \exp\left\{2\pi i t_n \left(f_d + a t_n/\lambda\right)\right\}, \qquad n = 1, 2, \ldots, N \tag{1}$$

where A_n are the return signal magnitudes governed by the radar range equation, λ is the radar wavelength, and $f_d = 2v_0/\lambda$ is the baseline target Doppler frequency corresponding to initial target velocity v_0. Here, n is an integer representing the sampling time index, N is the number of time samples in the CPI, or 'CPI length' as mentioned earlier. For simplicity, we also assume that signal reception is free of blind zones. The sampling rate for

each range bin , i.e. the inverse of the sampling period, also known as the pulse repetition frequency or 'PRF', determines the maximum unambiguous velocity of the system.

In this work, the target signal amplitudes A_n can be modelled as Swerling I type or Swerling II type. As a reminder, a Swerling I type target has a constant A_n for all values of n in a CPI, and for all CPIs of a time-on-target, but fluctuates according to a Chi-square distribution from scan to scan. Refer to [3] for more detail. On the contrary, a Swerling II type target signal has A_n varying pulse-to-pulse.

For the applications described herein, detection processing is required for each CPI, and the effects of scan-to-scan target fluctuation are not considered.

2.2   Clutter Model

The aim of this section is not to propose new clutter models but only to summarise the main features of well-known standard models which provide a necessary component of the composite radar backscatter signal, to which the novel tools of the FrFT and S-Method are applied.

The surface clutter model discussed here is derived from basic assumptions about the amplitude and Doppler distributions of the clutter backscatter of the surface, as described in [4]. As is customary in the radar clutter simulation community, the ground is usually represented by a number of 'patches' whose area is determined by the 'footprint' of the antenna main beam on the ground. If $\Delta\theta$ denotes the azimuth width of the main beam, which is also used as the clutter patch width, and Δr denotes the range bin size of the radar, then the area of a clutter patch is

$$A_c = r\,\Delta r\,\Delta\theta,$$

where r is the range to the patch. All such patches on the surface, indexed by a subscript i, contribute to the total clutter return, through either the mainlobe or the sidelobes of the antenna, depending on the instantaneous geometry. The signal from i^{th} patch can be modelled as

$$c_i(t) = C_i\,e^{i\phi_i(t)} \tag{2}$$

where C_i and ϕ_i respectively represent amplitude and phase of the signal, which are modelled separately as follows.

Clutter signal amplitude is modelled as a product of the area of the illuminated patch, denoted by A_{c_i}, and a backscatter coefficient called σ_i, i.e.

$$C_i = A_{c_i}\,\sigma_{0i}.$$

Furthermore, it is assumed that

$$\sigma_i = \sigma_{wi}\sigma_0,$$

where σ_0 models the mean reflection coefficient from the patch - a function of only radar frequency, grazing angle, and polarisation, while σ_w is a random variable with a Weibull distribution:

$$p(\sigma_0) = \alpha\,\beta\,\sigma_i^{\alpha-1}\,e^{-\beta\,\sigma_i^{\alpha}}. \tag{3}$$

Here, $\alpha = 1/a_i$, a_i is known as the shape parameter and β is known as the scale parameter.

Note that, for simplicity, we are assuming that the amplitude time samples from each patch are not correlated but are Weibull distributed across the different clutter patches.

The shape parameter is derived by the clutter cell area such that,

$$a_i = \begin{cases} \rho\,(A_{c_i}\,\psi_i)^{-1/3}, & \text{for sea clutter,} \\ 6.74 - 0.8\,\log_{10}(A_{c_i}), & \text{for land clutter,} \end{cases} \tag{4}$$

and $\rho = 3.75$ for horizontal polarisation and $\rho = 1.88$ for vertical polarisation.

The scale parameter is related to the mean reflection coefficient such that

$$\beta = \left\{ \frac{\Gamma(1 + a_i)}{\sigma_{0i}} \right\}^{1/a_i} \tag{5}$$

where $\Gamma(x)$ is the Gamma function of x.

The effectiveness of the signal to reflect off the surface is described by the mean reflection coefficient, σ_0, which depends only on the frequency, grazing angle and polarisation as mentioned earlier. The GIT model [6] and NECAPS model [4] are used for sea and land clutter mean reflection coefficient calculations respectively.

The phase function $\phi_i(t)$ of the clutter signal is modelled by simulating the instantaneous Doppler frequency of a clutter patch on the surface, which can be expressed in the form

$$f_i = f_p \cos\psi \cos\theta + f_{clut}$$

where ψ is the grazing angle (elevation angle between the radar and clutter patch), θ is the azimuth of the patch with respect to the radar, $f_p = 2v_p/\lambda$ is the platform Doppler (given a platform velocity of v_p), and $f_{clut} = 2v_i/\lambda$ is the statistical component of the clutter due to the surface characteristics, with v_i being a sample taken from a normal distribution with the mean and variance of the distribution depending on surface type.

For sea and land clutter, the mean of the distribution is,

$$\mu = \text{mean}(v_i) = \begin{cases} v_{dop}, & \text{for sea clutter,} \\ 0, & \text{for land clutter} \end{cases} \tag{6}$$

where

$$v_{dop} = \begin{cases} 0.85\,\sqrt{v_0}\,\cos\gamma, & \text{for horizontal polarisation,} \\ 0.15\,v_0\,\cos\gamma, & \text{for vertical polarisation} \end{cases} \tag{7}$$

where v_0 is the velocity of the clutter and γ is the angle between the platform direction and the wave direction. The variance is

$$\sigma^2 = \text{var}(v_i) = \begin{cases} 0.1\,v_0, & \text{for sea clutter,} \\ 0.5, & \text{for land clutter.} \end{cases} \tag{8}$$

The velocity of the sea clutter, v_0, is derived directly from the sea state [11], ss, where $v_0 = 3.16\,ss^{0.8}$. Finally, the time samples of the clutter signal phase function $\phi_i(t)$ for a CPI can be written as

$$\phi_i(t) = 2\pi(n-1)f_i \times PRI + \phi_0, \quad n = 1, 2, \ldots, N, \tag{9}$$

where PRI is the pulse repetition interval and ϕ_0 is the initial phase of the first pulse.

Table 1: *System and scenario parameters for clutter simulation*

Carrier Frequency, f_c	3 GHz
Pulse Repetition Freq, PRF,	40 kHz
Polarisation	horizontal
Platform Velocity, v_p	100 m/s
Antenna Look Direction	forward
Sea State, ss	3, 5
Wave Direction, γ	0°
Antenna Beamwidth, $\Delta\theta$	6°
Range Bin Size, Δr	150 m

2.2.1   An example

An example of simulated sea clutter using the model described above and typical scenario parameters is shown in Table 1. The clutter spectra for sea state 3 and 5 are shown in Figure 1, for which a CPI of 0.5 s is used. Note that:

1. Both mainlobe and sidelobe clutter are considered in these examples, employing a simple sinc antenna pattern, with sidelobe levels -13 dB below mainlobe. With a forward looking antenna, mainlobe clutter occurs at the upper edge of the clutter region, causing an asymmetric look to the clutter spectrum.

2. By the nature of our problem, only one range bin containing both mainlobe and sidelobe clutter is investigated with no clutter beyond the clutter patch. And for simplicity, only those clutter patches inside $\pm30°$ of the look angle are included.

3. Also for simplicity, and to investigate how clutter behaves under the FrFT, no noise is added to the simulated signal and no FFT windowing has been applied.
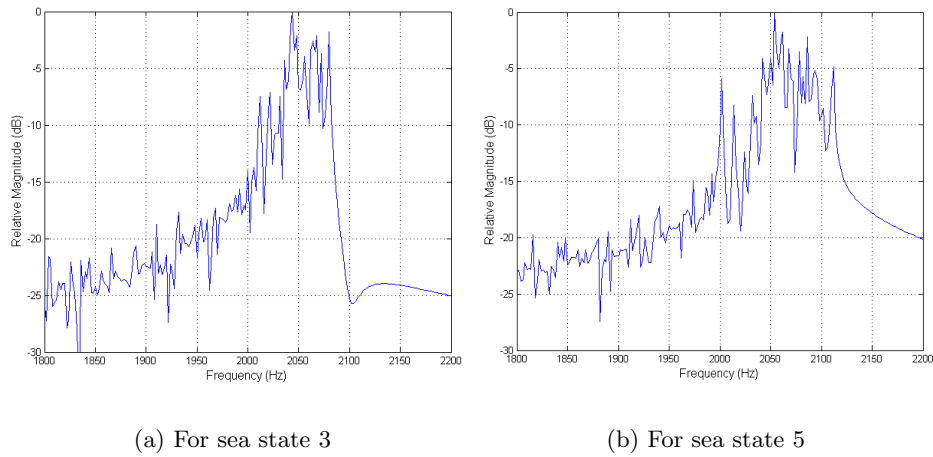

(a) For sea state 3   (b) For sea state 5

Figure 1: *Examples of Doppler spectra of simulated clutter for sea states 3 and 5, showing both mainlobe and sidelobe clutter.*

3   The Fractional Fourier Transform and The S-Method

The use of coherent integration techniques to detect signals contaminated by noise and/or clutter is older than radar itself. And in this area, the Fourier Transform (FT) and its discrete versions are pivotal. However, the FT works best only when the signal is made up of one or more pure tones. In radar detection problems, targets with an approximately constant velocity during a coherent integration time interval induce an approximately constant Doppler frequency, and hence are perfectly suited to the basic requirement of the FT. Beyond the assumption of constant velocity, coherency breaks down, though in a well defined manner, and the output from a FT processing is no longer a spectrum with well focused peaks, but may consist of smeared 'plateaus', such as that shown in Figure 2.
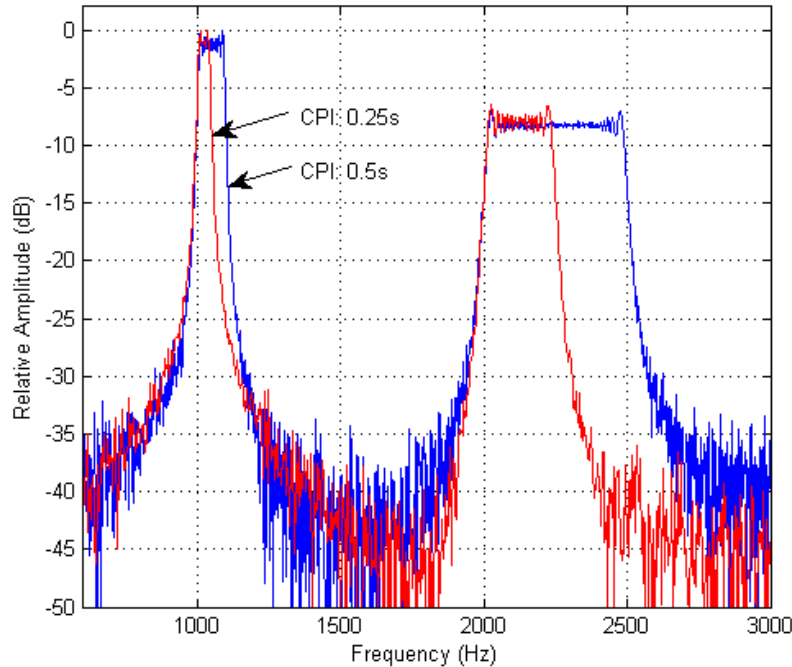

Figure 2: *The Fourier spectra of two chirp signals generated by scatterers with accelerations of $2g$ and $10g$ and the effect on the chirp bandwidth for different CPI's.*

The width of such a plateau is a measure of the bandwidth of the frequency modulated signal, or 'chirp'. Recently, Yasotharan *et al.* [7] have done a quantitative assessment of the degradation of the FT when applied to accelerating targets which typically produce a linear chirp during a CPI. An extension of the results contained in [7] are shown in Figure 3. The gain selected for plotting in this figure is the gain at the maximum point on the chirp. It can be seen that while the oscillatory behavior of the gain factor is the direct result of this choice for the gain factor, the mean gain factor quickly saturates, as the CPI length is increased, to a value that is monotonically decreasing with target acceleration.

The fractional Fourier transform (FrFT), first proposed by V. Namias [8], is a relatively new tool for signal processing. It can be described as a generalisation of the classic Fourier
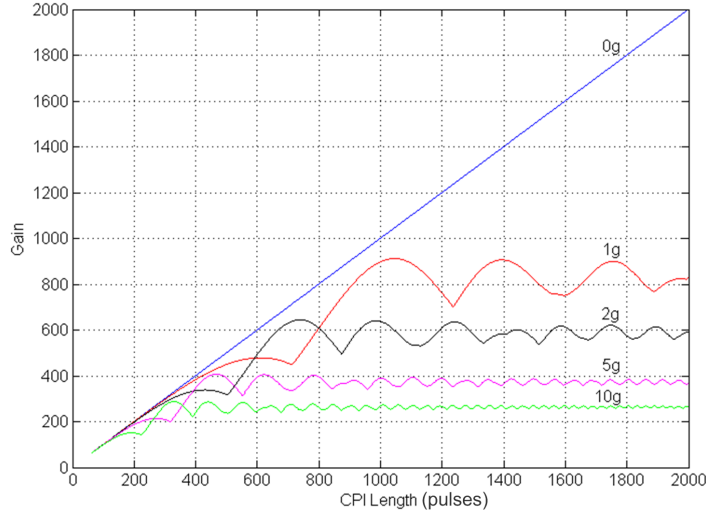
Figure 3: *Coherent gain of the traditional Fourier transform versus CPI length, for various target accelerations for a 3 GHz radar with a 40 kHz PRF.*

transform in which a linear chirp signal in the real time domain becomes a pure tone signal again in the suitably rotated time-frequency domain. An attractive advantage of the FrFT is that it is a linear transform, and hence is free from cross coupling between multiple frequency components of the signal. A disadvantage, however, is the extra computational cost associated with the search for the usually unknown chirp rate. For this reason, it is proposed in this work that the FrFT is used in conjunction with the S-Method form of Wigner distribution (WD) for detecting accelerating targets; the optimal precedence depends on specific target-clutter scenarios.

Techniques based on the WD or the S-Method have been proposed earlier in [1].[2] The advantage of the S-Method is its relatively low computational cost and high efficiency when a target is well separated from clutter, or if the S-Method is applied to the clutter clear region only. A possible disadvantage of the S-Method is with cross terms if multiple targets (multiple chirped signals) do exist in the same range bin, or if target-clutter separation is not available.

We postpone the discussion on the efficiency of applying these two techniques in real target detection scenarios to the next section. For the rest of this section, a brief summary of the theory and applications of the FrFT, the S-Method, along with measures of performance, are given.

---

[2]Though the authors therein considered a different problem.

3.1 The Fractional Fourier Transform

A definition of the FrFT is now given. For a time signal $s(t)$, its FrFT in continuous form is defined as

$$S_\alpha(u) = \mathcal{F}_\alpha\{s(t)\} = \int_{-\infty}^{\infty} K(\alpha, u, t)\, s(t)\, dt, \tag{10}$$

where the kernel function is

$$K(\alpha, u, t) = \begin{cases} \left(\frac{1 - i\cot\alpha}{2\pi}\right)^{1/2} \exp\{i\frac{\cot\alpha}{2}(u^2 + t^2)\} \exp\{-i\frac{u}{\sin\alpha}t\}, & \alpha \neq n\pi, \\ \delta(t - u), & \alpha = 2n\pi, \\ \delta(t + u), & \alpha = (2n - 1)\pi, \end{cases} \tag{11}$$

and where α is called the *order* of the transform, or 'transform order', which can also be interpreted as an angle of rotation in the time-frequency plane. For $\alpha = 0$ (i.e for $n = 0$ in Equation 11), we have $S_0(u) = s(u)$ which is the time-domain signal itself. For $\alpha = \pi/2$, we have $\cot\alpha = 0$ and $\sin\alpha = 1$, and $S_{\pi/2}(u)$ reduces to the traditional Fourier transform $S(u) = S(f)$ of $s(t)$. Indeed, the traditional FT can be insightfully interpreted as a rotation of the time signal through an angle of $\pi/2$ in the time-frequency plane. A rotation through some other angle gives a generalised or 'fractional frequency' spectrum of the signal at that angle, with the fractional frequency denoted[3] by u.

Properties of the FrFT and its numerical implementation have been summarised in [10] and the numerous references therein. Probably the most important effect to note is that, for the correct transform order α, the FrFT can achieve the maximum integration gain of N, which is the gain achievable by the traditional FT on a pure tone signal of N samples.

3.1.1 Application to accelerating targets

An accelerating target with constant (radial) acceleration a produces a constant chirp rate of $c_r = a/\lambda$, so that the instantaneous target Doppler frequency is $f = f_0 + c_r t$ where f_0 is an initial Doppler frequency. To spectrally compress such a chirp, the optimal transform order α that should be used is related to c_r through

$$\alpha = \frac{\pi}{2} + \beta = \frac{\pi}{2} + \tan^{-1}(D\, c_r), \tag{12}$$

in which the scale factor D due to the discretisation of the time-frequency domain is related to the time and frequency resolutions δt and δf by [12]

$$D = \left(\frac{\delta f}{\delta t}\right)^{-1} = \left(\frac{N}{PRF^2}\right). \tag{13}$$

Figure 4 illustrates the various quantities involved in (12). With an optimal rotation angle β as expressed in (12), the signal would appear like a 'pure tone' along the 'fractional time' domain, or equivalently as an optimally compressed spike in the 'fractional frequency' domain.

---

[3]For this reason, the same notation $\mathcal{F}$ is used for both the traditional Fourier transform and the fractional Fourier transform, with a subscript α explicitly denoting the 'fractional form'.
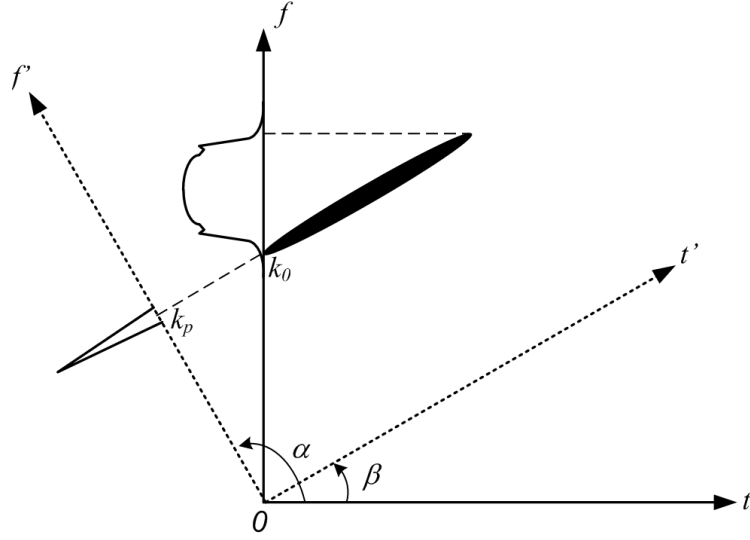
Figure 4: *A schematic illustration of the compression of chirped signals as the time-frequency plane is rotated and the relationship between pure Fourier domain and fractional Fourier domain.*

In real applications, true target acceleration a and hence c_r and α are generally unknown parameters to be estimated, and thus a search for optimum α is necessary. We use the following simple steps for this purpose:

1. The FrFT is applied for a range of α corresponding to realistically possible values of a, producing a 2-dimensional array of fractional frequency spectrum versus α. An example of such an array is shown in Figure 5.

2. The value of α producing the largest peak in this array, denoted by α_{opt}, is selected and the corresponding fractional frequency spectrum is extracted. If desired, a finer search around α_{opt} could be carried out for a more precise estimate of α.

3. The index of the initial (physical) frequency of the chirp signal is determined from the index of the fractional frequency of the largest peak, denoted by k_p, through the simple relation

$$k_0 = \frac{k_p}{\sin \alpha_{opt}}, \tag{14}$$

leading to an expression for the initial physical frequency, in Hz, of the chirp signal given by

$$f_0 = k_0 \frac{PRF}{N}. \tag{15}$$

A direct and perhaps more visual illustration of the performance of the FrFT relative to the traditional FT is shown in Figure 6. Note that the compressed frequency is not a physically meaningful frequency and in a filter not at the centre of the chirp plateau, but can be readily converted to physically meaningful quantities by relations (14) and (15).
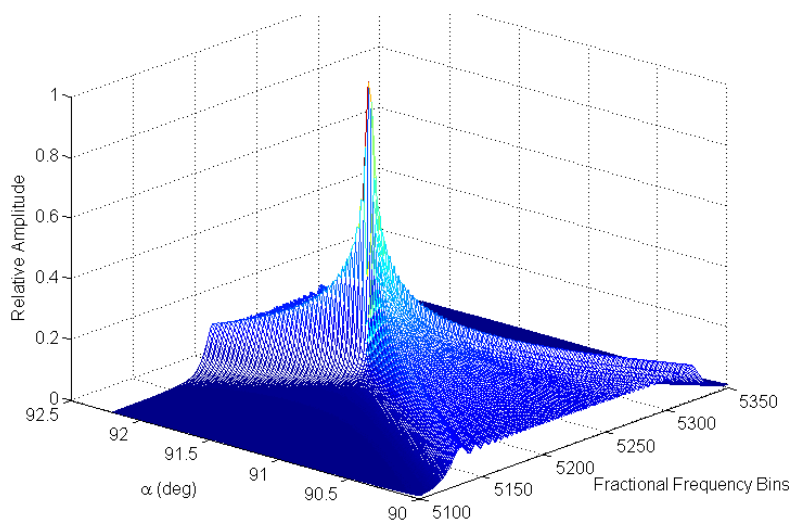
Figure 5: *The fractional Fourier spectra for a range of transform order α, with the traditional Fourier spectrum corresponds to $\alpha = 90°$.*
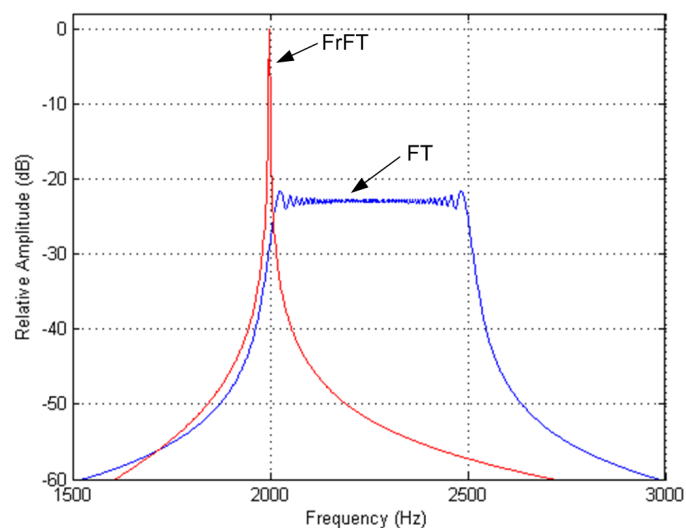

Figure 6: *The Fourier transform of a chirp and the equivalent fractional Fourier transform showing an improvement in relative amplitude due to the compressed spectrum.*

3.1.2   Effects of the FrFT on clutter

In this section, the effects of the FrFT on clutter is investigated, based on the surface clutter models described in Section 2.2.1. Clutter spectra for, for both sea and land clutter, as a function of α are shown in Figures 7(a), 7(b), and 7(c), which include the case of $\alpha = 90°$ (for the traditional FT). It should be noted that for each of the surface clutter cases, the clutter spectrum spreads out as α deviates from 90°. This effect may be due, at least in part, to the fact that the clutter model used here does not include second-moment effects suggesting that chirp-like characteristics in the data are not present, and hence clutter power would not be focused along the fractional frequency domain by the FrFT. However, if the spread of clutter is actually the case with real clutter, it would provide an extra advantage of using the FrFT: compressing chirp signals of interest while de-compressing the undesirable clutter. This issue will be investigated in a future work when real clutter data becomes available.

3.2   The S-Method

Of particular interest in the present study is the so-called S-Method, first proposed in L. Stankovic [9] in 1994. This tool is can be described as the Wigner distribution modified by a reduced integration extent, and is chosen for its relatively low computational cost and excellent performance when the component frequencies are well separated. In discrete form, the S-Method can be written as

$$S_{SM}(m,k) = \sum_{i=-L}^{L} S(m, k+i) \, S^*(m, k-i), \quad k = 1, 2, \ldots, N, \tag{16}$$

where m and n are respectively slow-time and frequency-filter indices; $S(m,k)$ with $k = 1, 2, \ldots, N$ is the discrete short-time Fourier transform (STFT) at m, and L is an integer chosen to minimize cross terms. When $L = 0$, the S-Method reduces to the spectrogram. When L spans the entire STFT domain, the S-Method is identical to the Wigner distribution. L can be chosen to vary with frequency filter index k, and since the aim is to optimise the focusing (or spectral compression) of the auto-terms and to avoid the cross terms, L needs to be determined adaptively for each value of n. In the present work, either of the following two criteria can be used for a 'simple hump' in the STFT: (1) the L-profile takes a triangular shape such that the sum in (16) stops when either $|S(m, k+i)|$ or $|S(m, k-i)|$ is less than a certain percentage of $|S(m,k)|$; or (2) the L-profile has a rectangular shape of sufficiently large height, which can be experimentally determined, extending just enough to cover the STFT hump to be compressed.

To facilitate a comparison with the FrFT, which is a linear transform, we modify slightly the conventional S-Method by taking the *square root* of the above sum and retrieve its first-order dimensionality:

$$S_{SM}(m,k) = \left[\sum_{i=-L}^{L} S(m, k+i) \, S^*(m, k-i) \right]^{1/2}. \tag{17}$$
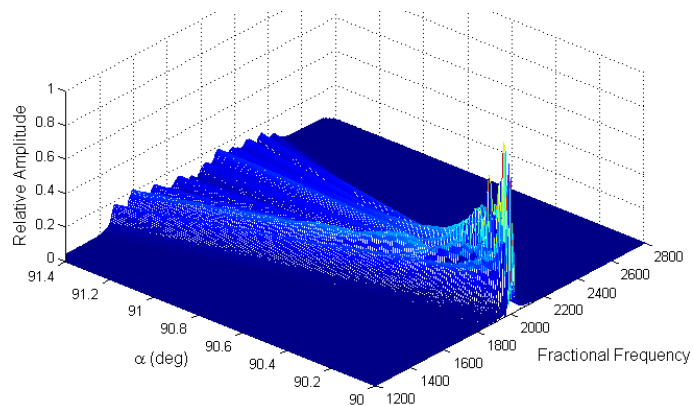
An important practical aspect of the S-Method is the *requirement of oversampling.* Accuracy of the discrete sum in (17) requires a certain minimum degree of oversampling
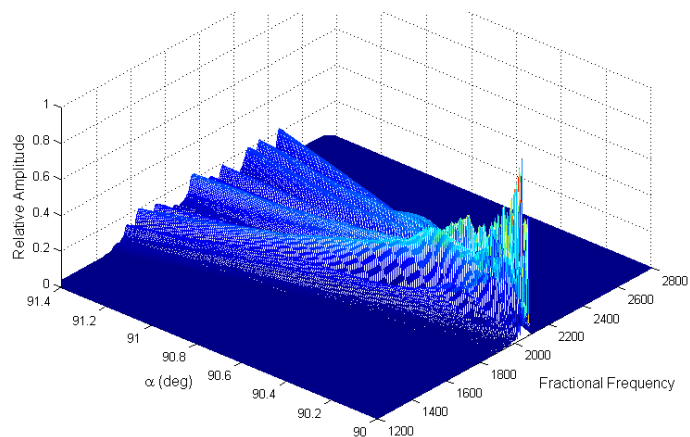
(a) Sea clutter spectra, sea state 3, for a range of transform order α
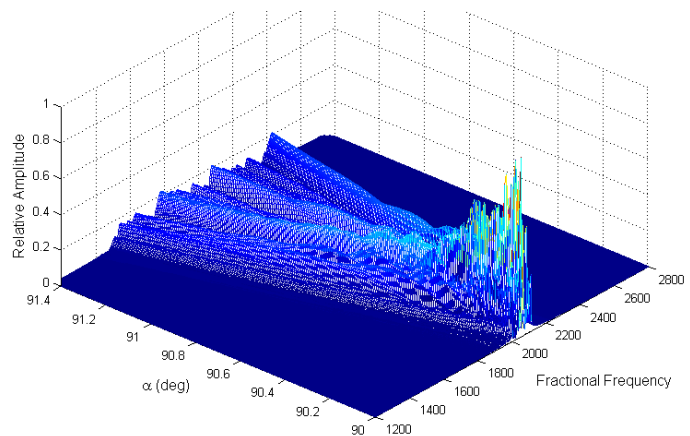
(b) Sea clutter spectra, sea state 5, for a range of transform order α

(c) Land clutter spectra for a range of transform order α

Figure 7: *Surface clutter spectra for a range of transform order α.*

in the time domain, which translates a certain degree of smoothing in the $S(m, k)$ array (in k). We have found by numerical experiments that a factor of at least 4 above the Nyquist sampling seems to be sufficient. This oversampling requirement adds to the computational cost of the S-Method.

Examples of applying the modified S-Method to typical chirp signals and clutter are shown in Figures 8(a) and 8(b) respectively. As expected, the S-Method spectrally compresses a LFM signal to that of a pure tone signal, while no compression is achieved for a clutter signal. An undesirable feature of the S-Method is also revealed in Figure 8(b): its inherent cross-term problem causes mainlobe clutter to 'leak' into the sidelobes, effectively raising sidelobe clutter levels which can potentially reduce detectability of targets of interest.
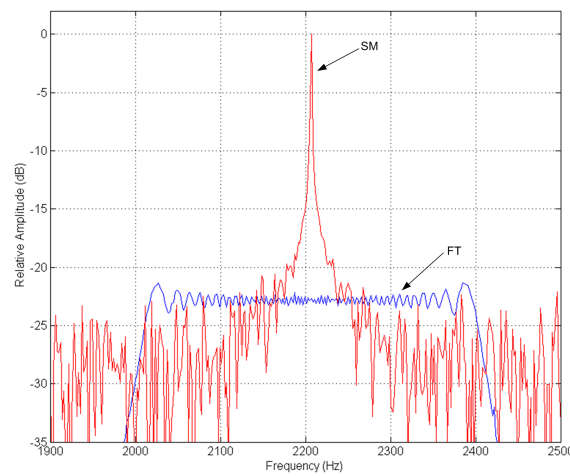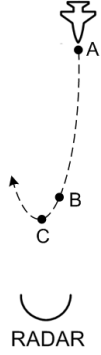
(a) Spectral compression by the S-Method on a LFM signal
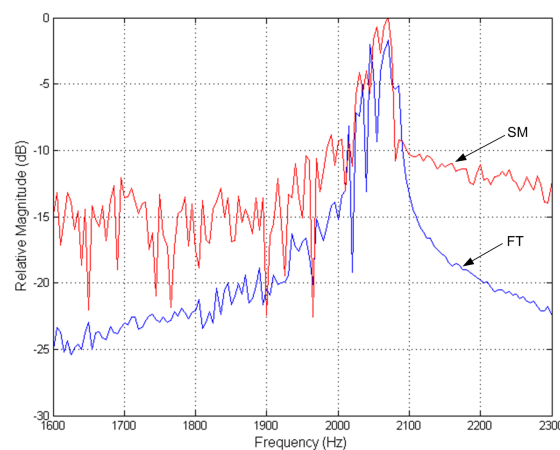
(b) S-Method on clutter of sea state 3

Figure 8: *The effect of the S-Method on a LFM signal and clutter.*

Location	Target velocity	Target Doppler
A	100 m/s	2 kHz
B	12 m/s	250 Hz
C	0 m/s	0 Hz

Figure 9: *Target trajectory and Doppler characteristics at 3 particular locations considered.*

4   Results

In this section we aim to apply the FrFT and S-Method techniques to investigate the enhanced coherent integration of a target signal in a clutter environment, for a range of target acceleration, CPI length, and for a typical value of the signal-to-clutter ratio (SCR). A typical target manoeuvre is used which captures typical locations of the target relative to clutter in the Doppler frequency domain: target in the clutter-free region, near the clutter edge, and well inside the clutter region.

The maximum achievable coherent integration gain for the FrFT and the S-Method is still N, the number of samples used in a CPI. In digital implementation, however, the actual gain may be slightly less than N due to target Doppler frequency straddling between discrete filters. It is thus meaningful to use N as a 'bench mark' to measure the performance. It is also useful to compare it with the gain by the traditional FT. For consistency, we define integration gain as follows. For a well-defined peak, gain is set equal to the magnitude of the peak. For a spread chirp spectrum, gain is set equal to the averaged amplitude of the 'plateau region' of the spectrum.

4.1   Scenario and System Description

For a demonstration, we use the following simulated scenario and system setup. A pulse Doppler radar operating at a frequency of 3 GHz, with a pulse repetition frequency of 40 kHz, horizontal polarisation, is mounted on a platform travelling at 100 m/s. A target, approaching the radar platform, nose aspect, at a constant (negative) acceleration a, and makes a U-turn manoeuvre, as depicted in Figure 9. The target locations, at which we wish to investigate target detection processing, are labeled as A, B, and C, at which target velocities and Doppler frequencies are as listed in the table in Figure 9. The clutter environment includes both land and sea clutter using the clutter models and parameters described in Section 2.2. It should be noted that for locations B and C, only the FrFT processing is applicable, as discussed in Section 3.2.

At location A, the approaching and accelerating target produces a spread Doppler plateau that is well clear of the clutter region, as shown in Figure 10(a). After FrFT

processing, the resulting spectrum, shown in Figure 10(b), shows a well compressed spike for the target and a spread-out region for the clutter which is also attenuated by about 15 dB below the target spike.

Similar performance results by the FrFT are can be seen at location B in Figures 10(c) and 10(d), at which the target manoeuvres such that its Doppler content partially overlaps with that of clutter, and for location C in Figures 10(e) and 10(f) at which the mean target velocity is zero but target acceleration is non-zero and is the same as at locations A and B. Regardless of the relative locations of the target and clutter in the frequency domain, whether target is well clear of clutter or totally inside clutter, the FrFT always optimally enhances the target signal while attenuating the clutter signal at the same time.

To demonstrate the effect of the S-Method on the signal and clutter, the spectra for an accelerating target and clutter at locations A, B and C is shown in Figure 11. For location A, the spectra for clutter and target signal processed using the S-Method are well separated in Doppler, as seen in Figure 11(a), making the S-Method effective at compressing the chirped signal. However, the S-Method involves data outside the target Doppler region giving rise to leakage of noise into the S-Method processing. Hence, the overall signal-to-noise ratio is increased and is inferior to the FrFT processing seen in Figure 10(b).

For similar reasons, the S-Method performance is greatly degraded when the target Doppler overlaps the clutter region, as for locations B and C seen in Figures 11(b) and 11(c), with no improvement in signal gain compared with the FrFT processing for the relative locations.

4.2   Comparison Results

In this section, the performance of the FrFT and the S-Method on accelerating targets compared with the traditional FT is investigated. A signal is generated such that the signal-to-clutter ratio (SCR) is set to 5 dB and the clutter-to-noise ratio (CNR) is set at 10 dB. For each of the target locations, the integration gain produced from the FrFT and FT is presented as a function of CPI length, for various target accelerations. The S-Method results are included for location A only. Also, for comparison purposes, the FT of a non-accelerating target is presented as this represents the maximum integration gain possible for a given CPI length.

At location A, the integration gain as a function of CPI length, for various values of target acceleration, is shown in Figure 12. When the target Doppler is well clear of the clutter Doppler, both the FrFT and S-Method compare closely with a non-accelerating target, for each of the target accelerations cases. Figure 13 and 14 show the results for the FrFT as compared to the FT for locations B and C respectively. Again, the FrFT processing achieves results that are similar to the non-accelerating target case for each of the target accelerations, even when the target is obscured by clutter.
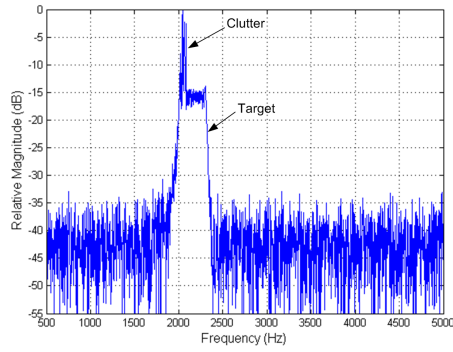
These results convincingly demonstrate that the FrFT is robust for detection of an accelerating target in both land and sea clutter, at least for simulated clutter.
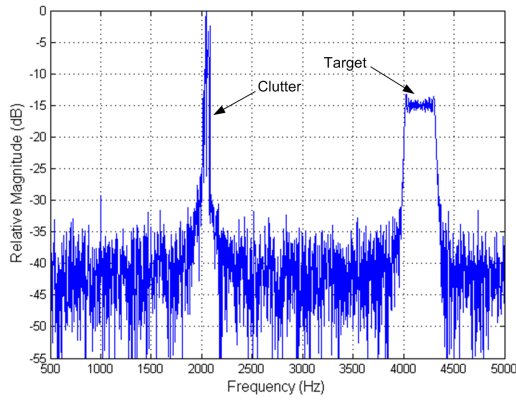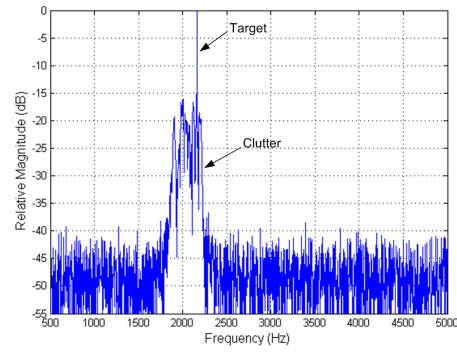
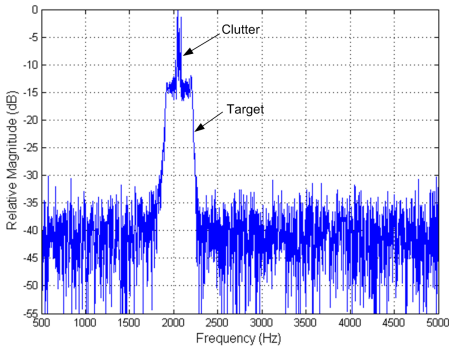(a) Spectra showing accelerating target and clutter Dopplers for location A
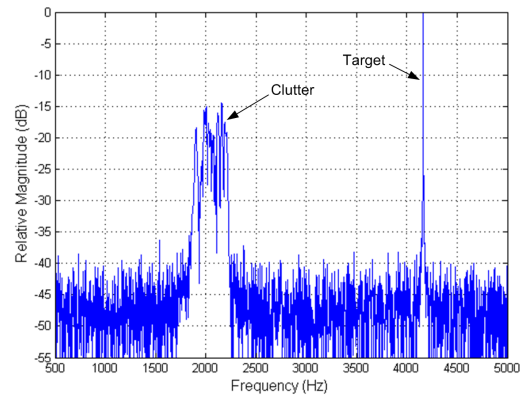
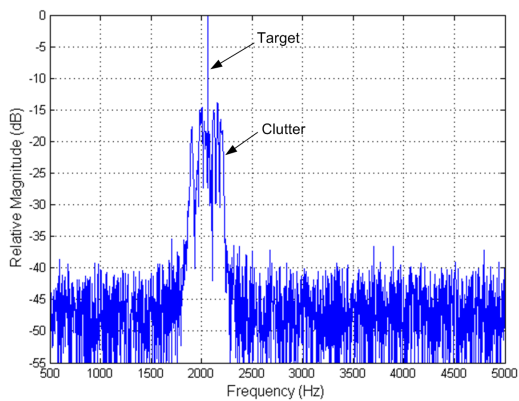(b) Same as (a), after FrFT processing

(c) Spectra showing accelerating target and clutter Dopplers for location B
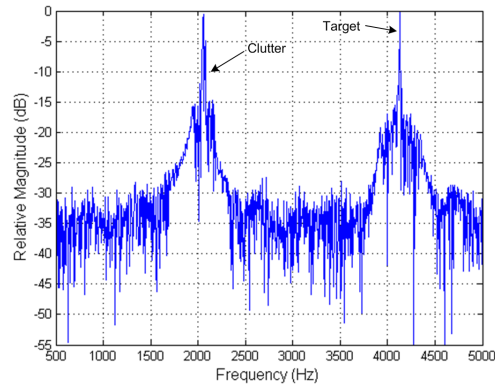
(d) Same as (c), after FrFT processing

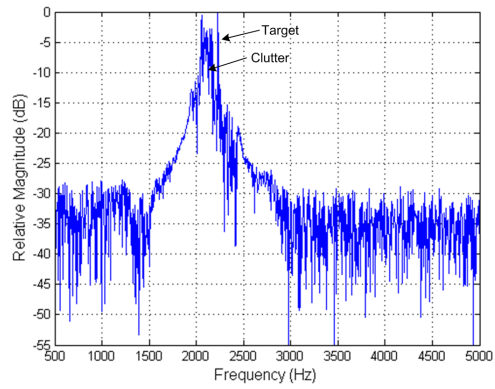(e) Signal spectra showing accelerating target and clutter Dopplers for location C

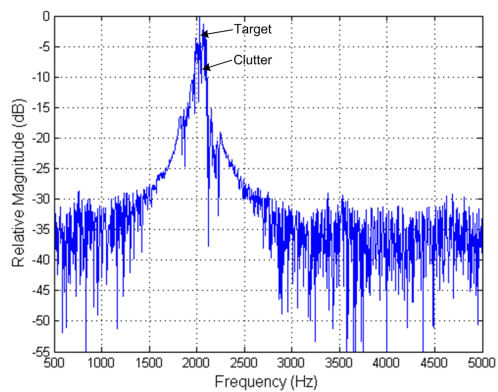(f) Same as (e), after FrFT processing

Figure 10: *Spectra of clutter and an accelerating target signals at locations A, B, and C, for a 3 GHz radar with 40 kHz PRF, on a platform travelling at 100 m/s. Left figures: FT processed; right figures: FrFT processed. Plots normalised to peak signal.*

(a) Spectra showing accelerating target and clutter Dopplers for location A

(b) Spectra showing accelerating target and clutter Dopplers for location B
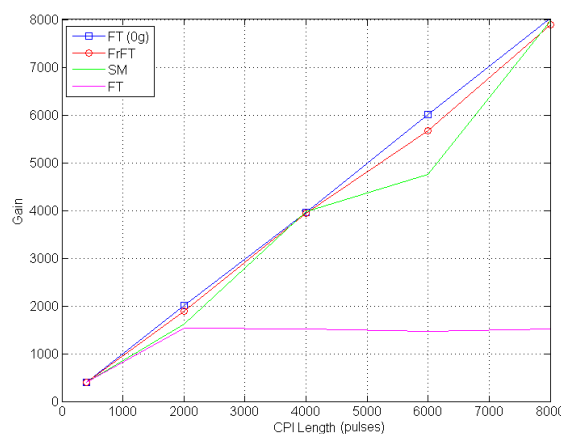

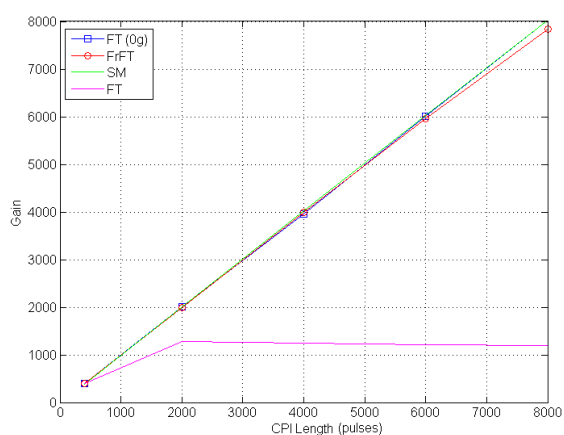(c) Spectra showing accelerating target and clutter Dopplers for location C

Figure 11: Spectra of clutter and an accelerating target signals at locations A, B, and C, for a 3 GHz radar with 40 kHz PRF, on a platform travelling at 100 m/s, processed using the S-Method. Plots normalised to peak signal.
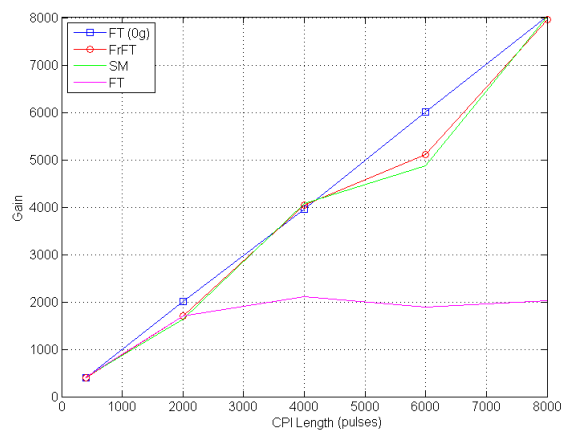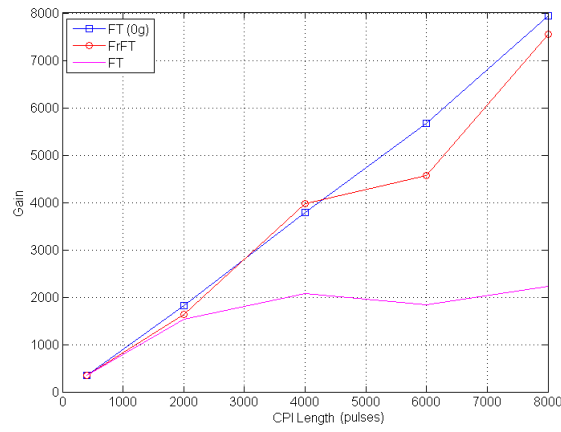
(a) Target acceleration of 3g
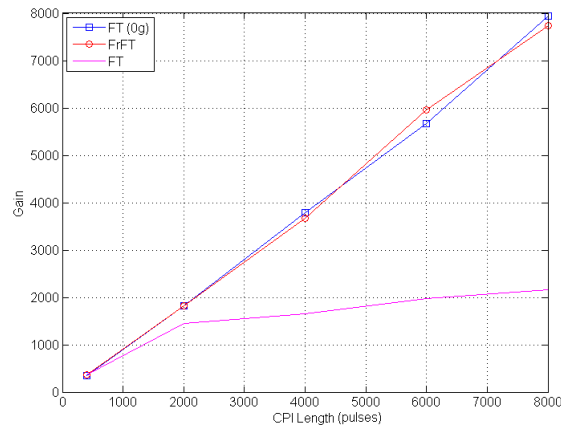

(b) Target acceleration of 5g
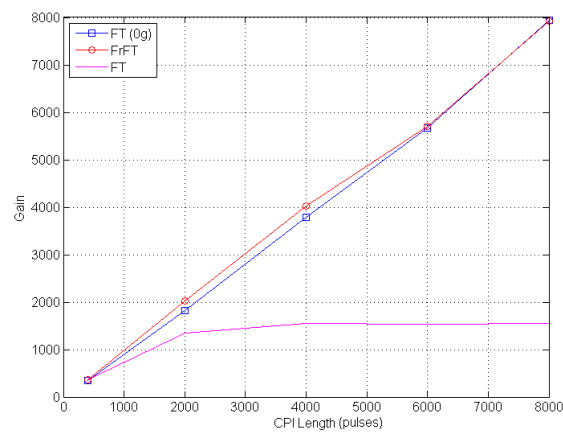

(c) Target acceleration of 8g

Figure 12: *Processing gain as a function of CPI length, at 40 kHz PRF, 3 GHz carrier frequency, for the target at location A (mean inbound velocity of 100 m/s) for various accelerations.*

(a) Target acceleration of 3g

(b) Target acceleration of 5g

(c) Target acceleration of 8g

Figure 13: *Processing gain as a function of CPI length, at 40 kHz PRF, 3 GHz carrier frequency, for the target at location B (mean inbound velocity of 12 m/s) for various accelerations.*
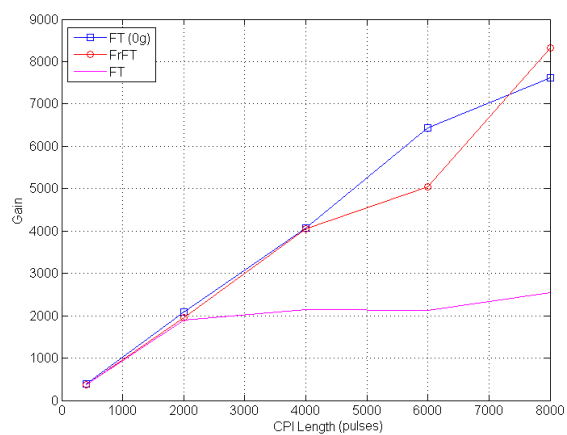
(a) Target acceleration of 3g
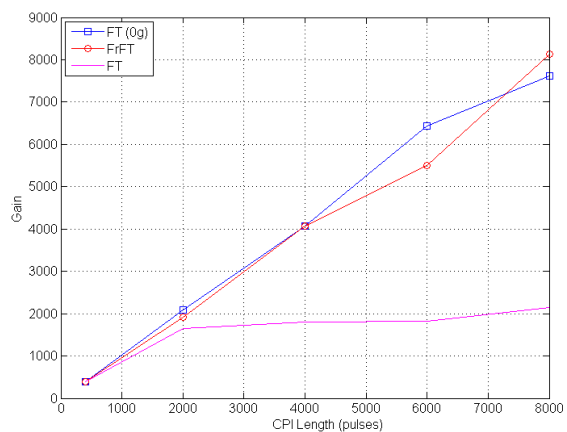
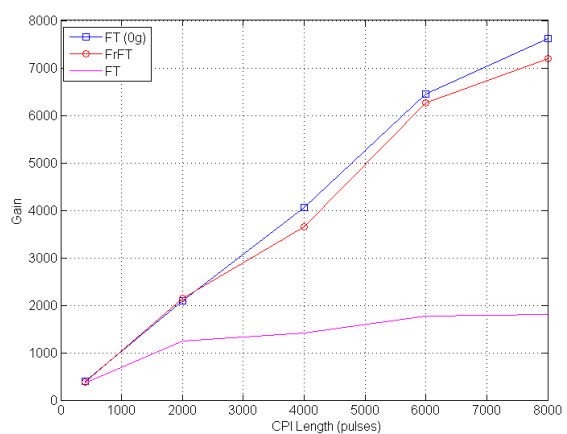(b) Target acceleration of 5g

(c) Target acceleration of 8g

Figure 14: *Processing gain as a function of CPI length, at* 40 *kHz PRF,* 3 *GHz carrier frequency, for the target at location C (mean inbound velocity of* 0 *m/s) for various accelerations.*

5   Conclusion

We have shown that both the S-Method and the FrFT are useful tools for detecting accelerating targets, where the traditional Fourier transform fails. However, the FrFT proves more practical when target detection must be achieved against a clutter background. For each processing technique the maximum coherent integration gain as in the case for the Fourier transform on pure tone signals can almost be achieved. Also, the nature of the FrFT processing suppresses clutter in the fractional frequency domain increasing the clutter-to-signal ratio which is already enhanced from the FrFT integration gain.

Our investigation will be extended to include an accelerating target using real clutter data in a future report, which will also delve further into the suppression effects of the FrFT on real clutter.

Acknowledgements

References

1. Yasotharan A., and Thayaparan T., *"Time-frequency method for detecting an accelerating target in sea clutter"*, IEEE Transactions on Aerospace and Electronic Systems, Vol 42, No.4, October 2006, pp.1289-1310.

2. Thayaparan T., and Kennedy S., *"Application of joint time-frequency representations to a maneuvering air target in sea clutter: Analysis beyond FFT"*, DRDC Technical Memorandum, TM 2003-090, March 2003.

3. Swerling, P., *"Probability of detection for fluctuating targets"*, The RAND Corporation, Research Memorandum RM-1217, March 17, 1954.

4. Defence Evaluation and Research Agency UK, *"Naval Environmental Clutter, Attenuation and Propagation Specification - NECAPS 3"*, DERA/SS/CS/WP000023/1.0.

5. Skolnik, M., *"Radar handbook, 2nd edition"*, McGraw-Hill, 1990

6. Horst, M., Dyer,F., and Tuley,M., *"Radar sea clutter model"*, International Conference on Antennas and Propagation. IEE. Part II, pp. 6-10. London, UK., 1978.

7. Yasotharan A., and Thayaparan T., *"Strengths and limitations of the Fourier method for detecting accelerating targets by pulse Doppler radar"*, IEE Proceedings - Radar Sonar Navigation, Vol 149, No.2, April 2002, pp.83-88.

8. Namias, V., *"The fractional Fourier transform and its application to quantum mechanics"*, J. Inst. Math. Appl., Vol.25, pp.241-65, 1980.

9. Stankovic L., *"A method for time-frequency analysis"*, IEEE Transactions on Signal Processing, Vol.42, No.1, Jan 1994, pp.225-9.

10. Tran H.T., and Melino R., *"Application of the fractional Fourier transform and S-method in Doppler radar tomography"*, DSTO Research Report, DSTO-RR-0357, August 2010.

11. Huizing, A.G., and Theil, A., *"CARPET: Radar performance analysis software and users manual version 1.0"*, Artech House, 1993.

12. Capus, C., *"Short-time fractional Fourier methods for the time-frequency representation of chirp signals"*, Journal of Acoustical Society of America, Vol. 113, No. 6, June 2003.

DEFENCE SCIENCE AND TECHNOLOGY ORGANISATION DOCUMENT CONTROL DATA	1. CAVEAT/PRIVACY MARKING

2. TITLE	3. SECURITY CLASSIFICATION		
Application of the Fractional Fourier Transform in the Detection of Accelerating Targets in Clutter	Document	(U)	
	Title	(U)	
	Abstract	(U)	

4. AUTHORS	5. CORPORATE AUTHOR
R. Melino and H.T. Tran	Defence Science and Technology Organisation PO Box 1500 Edinburgh, South Australia 5111, Australia

6a. DSTO NUMBER	6b. AR NUMBER	6c. TYPE OF REPORT	7. DOCUMENT DATE
DSTO–RR–0365	014–960	Research Report	April, 2011

8. FILE NUMBER	9. TASK NUMBER	10. TASK SPONSOR	11. No. OF PAGES	12. No. OF REFS
2010/1178180/1			22	12

13. URL OF ELECTRONIC VERSION	14. RELEASE AUTHORITY
http://www.dsto.defence.gov.au/ publications/scientific.php	Chief, Electronic Warfare and Radar Division

15. SECONDARY RELEASE STATEMENT OF THIS DOCUMENT
Approved for Public Release
OVERSEAS ENQUIRIES OUTSIDE STATED LIMITATIONS SHOULD BE REFERRED THROUGH DOCUMENT EXCHANGE, PO BOX 1500, EDINBURGH, SOUTH AUSTRALIA 5111

16. DELIBERATE ANNOUNCEMENT
No Limitations

17. CITATION IN OTHER DOCUMENTS
No Limitations

18. DSTO RESEARCH LIBRARY THESAURUS
Fractional Fourier Transform S-Method Wigner Distribution Time-Frequency Techniques Radar Target Detection Accelerating Target Chirped Signals Radar Clutter Clutter Suppression

19. ABSTRACT
We demonstrate that the Fractional Fourier transform is a very efficient and practical technique for detecting accelerating targets in both land and sea clutter, where the traditional Fourier transform method may fail.